EUROPEAN ORGANIZATION FOR NUCLEAR RESEARCH

CERN-EP/89-152
November 17th, 1989

SEARCH FOR TOP QUARK PRODUCTION AT THE CERN $\bar{p}p$ COLLIDER

The UA2 Collaboration

Bern - Cambridge - CERN - Heidelberg - Milano -
Orsay (LAL) - Pavia - Perugia - Pisa - Saclay (CEN)

T.Åkesson[6], J.Alitti[10], R.Ansari[6], R.E.Ansorge[2], P.Bagnaia[3,a], P.Bareyre[10], G.Blaylock[3], P.Bonamy[10], M.Bonesini[5,3], K.Borer[1], D.Buskulic[6], G.Carboni[9], D.Cavalli[5], V.Cavasinni[9], P.Cenci[8], J.C.Chollet[6], C.Conta[7], G.Costa[5], F.Costantini[9,3], A.Dell'Acqua[7], B.De Lotto[7,b], T.Del Prete[9], R.S.DeWolf[2], L.Di Lella[3], G.F.Egan[3,c], K.F.Einsweiler[3], L.Fayard[6], A.Federspiel[1], R.Ferrari[7], M.Fraternali[7,d], D.Froidevaux[6], G.Fumagalli[3,7], J.M.Gaillard[6], F.Gianotti[5], O.Gildemeister[3], C.Gössling[3,e], V.G.Goggi[7,3], S.Grünendahl[4], J.R.Hansen[3], K.Hara[1,f], S.Hellman[3], E.Hugentobler[1], K.Hultqvist[3], E.Iacopini[9,g], J.Incandela[3], K.Jakobs[3], P.Jenni[3], E.E.Kluge[4], N.Kurz[4], S. Lami[9], P.Lariccia[8], M.Lefebvre[2,3], L.Linssen[3], M.Livan[7,h], P.Lubrano[3], C.Magneville[10], L.Mandelli[5], L.Mapelli[3], M.Mazzanti[5], K.Meier[3], B.Merkel[6], J.P.Meyer[10], M.Moniez[6], R.Moning[1], M.Morganti[9,i], L.Müller[1], D.J.Munday[2], C.Onions[3], T.Pal[3,1], M.A.Parker[3], G.Parrour[6], F.Pastore[7], E.Pennacchio[7], J.M.Pentney[2], M.Pepe[8], L.Perini[5,d], C.Petridou[9], P.Petroff[6], H.Plothow-Besch[4], M.Primavera[9,j], G.Polesello[5,3], A.Poppleton[3], L.Rasmussen[3], J.P.Repellin[6], A.Rimoldi[7], J.G.Rushbrooke[2,k], P.Scampoli[8], J.Schacher[1], S.L.Singh[2], S.Stapnes[3], A.V.Stirling[10], S.N.Tovey[3,c], G.Unal[6], M.Valdata-Nappi[9,j], V.Vercesi[3,7], A.R.Weidberg[3], P.S.Wells[2], T.O.White[2], D.R.Wood[3], S.A.Wotton[2], H.Zaccone[10]

(submitted to Zeitschrift für Physik C)

ABSTRACT

The upgraded UA2 detector has collected data corresponding to a total integrated luminosity of 7.5 pb^{-1} from $\bar{p}p$ collisions at a centre of mass energy of 630 GeV during 1988 and 1989. A search has been performed for the production and decay of the top quark (t) or a member of a hypothetical fourth family (b'). No evidence has been found for such processes. Using the expected rates for production and decay branching ratios from the Standard Model, this implies that the top quark mass is greater than 69 (71) GeV/c^2, and that the b' mass is greater than 54 (57) GeV/c^2, at 95 (90)% confidence.

1 Laboratorium für Hochenergiephysik, Universität Bern, Sidlerstraβe 5, 3012 Bern, Switzerland
2 Cavendish Laboratory, University of Cambridge, Cambridge, CB3 0HE, UK
3 CERN, 1211 Geneva 23, Switzerland
4 Institut für Hochenergiephysik der Universität Heidelberg, Schröderstraβe 90, 6900 Heidelberg, FRG
5 Dipartimento di Fisica dell'Università di Milano and Sezione INFN Milano, 20133 Milano, Italy
6 Laboratoire de l'Accélérateur Linéaire, Université de Paris-Sud, 91405 Orsay, France
7 Dipartimento di Fisica Nucleare e Teorica, Università di Pavia and INFN, Sezione di Pavia, Via Bassi 6, 27100 Pavia, Italy
8 Dipartimento di Fisica dell'Università di Perugia and INFN, Sezione di Perugia, via Pascoli, 06100 Perugia, Italy
9 Dipartimento di Fisica dell'Università di Pisa and INFN, Sezione di Pisa, Via Livornese, S.Piero a Grado, 56100 Pisa, Italy
10 Centre d'Etudes Nucléaires de Saclay, 91191 Gif-sur-Yvette Cedex, France
a) Now at Dipartimento di Fisica, Università di Roma, Italy
b) Now at Dipartimento di Fisica, Università di Udine, Italy
c) Visitor from the University of Melbourne, Parkville, Australia 3052
d) Now at Dipartimento di Fisica, Università di Palermo, Italy
e) Now at Institut für Physik, Universität Dortmund, FRG
f) Now at University of Tsukuba, Tsukuba, Ibaraki 305, Japan
g) Also at Scuola Normale Superiore, Pisa, Italy
h) Now at Dipartimento di Fisica, Università di Cagliari, Italy
i) Now at Dipartimento di Fisica e INFN di Bologna, Università Bolognia, Italy
j) Now at Dipartimento di Fisica dell'Università della Calabria, Cosenza, Italy
k) Now at Bond University, Gold Coast, Queensland, Australia 4217

1. INTRODUCTION

The Standard Model of electroweak interactions requires that each quark family consists of left-handed fields forming doublets under SU(2) and right-handed singlet fields. The classification of quarks as left-handed weak isospin doublets prevents various processes, notably flavour-changing neutral currents, from occuring at rates in contradiction to experiment. Given the existence of the bottom quark (b), the Standard Model implies that its partner, the top (t), must also exist. Calculations [1] indicate that its mass must be less than ≈ 200 GeV/c^2, if the model is to remain consistent with the body of experimental data.

Experimental searches at e^+e^- machines[2] and at hadron colliders [3] have failed to find any evidence for the top quark with a mass lower than 41 GeV/c^2 at the 95% confidence level.

The upgraded UA2 detector has been used to search for the signature of top quark production and semi-electronic decay in $\bar{p}p$ collisions at a centre of mass energy $\sqrt{s} = 630$ GeV. A data sample of total integrated luminosity 7.5 pb^{-1} was collected during the 1988 and 1989 runs of the CERN $\bar{p}p$ collider thanks to the successful construction and operation of the new Antiproton Accumulator Complex (AAC), which enabled the collider to run at peak luminosities of up to $3 \cdot 10^{30}$ $cm^{-2}s^{-1}$.

In the following sections the mechanism for top production and decay at the $\bar{p}p$ collider is discussed. The main features of the UA2 apparatus relevant to this analysis are given, and the cuts used to select the data sample are explained. Estimates of the rates of signal and various backgrounds are then presented, and compared with the observations in order to extract upper limits on the cross section for top production. These are then used to infer a lower limit on the mass of the top quark, and on the mass of a possible b' quark from an as yet undiscovered quark family.

2. TOP PRODUCTION AND DECAY

Top quarks could be produced at the $\bar{p}p$ collider from two dominant processes, either mediated by the weak interaction ($t\bar{b}$) :

$$\bar{p}p \rightarrow W + X \; ; \; W \rightarrow t\bar{b} \text{ or } \bar{t}b \qquad (1) \, ,$$

or by the strong interaction ($t\bar{t}$) :

$$\bar{p}p \rightarrow t\bar{t} + X \qquad (2) \, .$$

The number of top quarks produced by reaction (1) can be computed as :

$$N_{top} = 3 \int Ldt\, \sigma(\bar{p}p \rightarrow W \rightarrow e\nu_e)\, PS(m_t)\, F_{QCD}\,,$$

where the factor 3 relates the production of coloured quarks to leptons, $\int Ldt$ is the integrated luminosity used in this analysis (7.1 ± 0.5 pb^{-1}), $PS(m_t)$ is a phase-space factor depending on the top quark mass, and F_{QCD} is a correction for higher order QCD processes, which becomes important if the top quark mass is close to that of the W boson. For example, for a W mass of 80.2 GeV/c^2 and a top quark mass of 65 GeV/c^2, $F_{QCD} = 1.5$ [5]. Since this correction is determined from an incomplete theoretical calculation, it was set equal to the conservative value of 1.0 in this analysis, and only the well understood lowest order calculation was used to estimate the rate of top production. From the total number of reconstructed $W \rightarrow e\nu_e$ decays in UA2, N_W, we can derive a preliminary cross section times branching ratio [4] :

$$\sigma(\bar{p}p \rightarrow W \rightarrow e\nu_e) = 630 \pm 20(\text{stat.}) \pm 50(\text{syst.})\ \text{pb}\,.$$

The uncertainty on the estimate of N_{top} was mainly due to the statistical uncertainty on N_W, since the systematic error on $\sigma(\bar{p}p \rightarrow W \rightarrow e\nu_e)$ is dominated by the uncertainty on the integrated luminosity, which cancels when computing N_{top}. The dependence of the W width on the top mass was taken into account. The cross section (including the phase space factor) is shown in Fig. 1.

The cross section for reaction (2) has been evaluated [6] using the full next-to-leading order calculation of Ref. [7]. The result is shown in Fig. 1 as a band indicating the theoretical uncertainties. For top quark masses between 35 and 70 GeV/c^2, top quark production is dominated by the electroweak $t\bar{b}$ production process at $\sqrt{s} = 630$ GeV.

Decays of the top quark into final states containing only hadronic jets are very difficult todistinguish from the large background due to QCD processes. The search was therefore performed using the decay mode :

$$t \rightarrow be\nu_e\,,$$

which has a branching ratio of approximately 1/9 in the Standard Model. In this case, the signature of top quark production consists of events containing an electron, one or more hadronic jets from the associated t or b quarks, and a transverse momentum imbalance (missing p_T) due to the neutrino produced in the top decay. Because of the high top quark masses considered here, the electron and jets will be produced preferentially in the central region, in contrast to most background processes. Accordingly, only electron candidates in the central calorimeter were considered in this analysis.

3. THE UA2 APPARATUS

The UA2 detector was upgraded during the period 1985 to 1987. Details of the construction and performance of the various detector elements can be found in the references given below. Only the main features relevant to this analysis will be summarised here.

3.1 Calorimetry

A partial longitudinal view of the UA2 calorimeters is shown in Fig. 2. The original UA2 central calorimeter [8] was retained with minor modifications. It covers the full azimuthal range, $0° < \phi < 360°$ and polar angles $40° < \theta < 140°$. Each of the 240 electromagnetic and hadronic cells subtends $10°$ in θ and $15°$ in ϕ. The electromagnetic part is a multi-layer sandwich of lead and scintillator, 17 radiation lengths thick, while the hadronic part is an iron-scintillator sandwich, giving a thickness of 4.5 absorption lengths including the electromagnetic cells. For the upgrade all the scintillator plates of the two hadronic compartments were replaced and, in order to increase the radial space available for the new central detector, the thickness of the electromagnetic compartments of the edge cells was reduced.

The end cap calorimeters (end-caps) [9] cover the pseudorapidity region $1 < |\eta| < 3$. Each end-cap consists of 12 modules and each module is segmented into 16 cells. In a given module the two cells closest to the beam axis ($2.5 < |\eta| < 3.0$ and $2.2 < |\eta| < 2.5$) cover $30°$ in azimuth. The other cells have a constant segmentation of $\Delta\phi = 15°$, $\Delta\eta = 0.2$. All the cells in the pseudorapidity interval $1.0 < |\eta| < 2.5$ have one electromagnetic and one hadronic compartment. The electromagnetic compartment is a multi-layer sandwich of lead (3 mm thick) and acrylic scintillator (4 mm thick), with a total thickness varying from 17.1 to 24.4 radiation lengths depending on the polar angle. The hadronic compartment is a multi-layer sandwich of iron (25 mm thick) and scintillator (4 mm thick) corresponding to ~ 6.5 absorption lengths, including the electromagnetic compartments. The cells nearest to the beam have only a hadronic compartment. In addition, cells with only a hadronic compartment cover the pseudorapidity interval $0.9 < |\eta| < 1.0$ to measure particles escaping from the interface between the end-cap and the central calorimeters (see Fig. 2). Each compartment is read out via two wave-length shifting plates placed on the opposite azimuthal sides of each cell, introducing a dead space between adjacent cells of 7 mm for the electromagnetic compartments and of 13 mm for the hadronic ones. To minimise the effect of these dead spaces each module is rotated by 50 mrad around its symmetry axis normal to the beam.

Clusters of deposited energy were formed in the calorimeters by joining all cells with an energy transverse to the beam direction greater than 400 MeV sharing a common edge. Clusters with a small lateral size and a leakage into the hadronic compartments consistent with a shower from a single electron were marked as electromagnetic.

Since the response of the calorimeter to hadronic showers depends on the fraction of the energy carried by hadrons, a correction factor was defined for each compartment of the calorimeter, and was applied to the observed energies in hadronic showers in order to compensate for the difference in response. The calorimeter correction factors applied to the electromagnetic cells were 1.18 in the central calorimeter and 1.20 in the end caps. A correction factor of 1.06 was also applied to energies observed in the second hadronic compartment of the central calorimeter, to account for energy leaking through the back of the calorimeter.

The efficiency for finding an electromagnetic cluster from an electron candidate with an energy flow transverse to the beam direction, $E_T > 12$ GeV, was measured from test beam data to be $\varepsilon_{cal} = 91.3 \pm 2.0\%$, in the central calorimeter, averaging over all the allowed impact directions for electrons. The main loss was of electrons which struck inter-cell boundaries or the shortened electromagnetic cells at the edge of the calorimeter, giving a large hadronic leakage.

3.2 The Central Detector

The layout of the central detector is shown in Fig. 2. Around the beryllium beam-pipe, at radii of 3.0 cm and 14.5 cm, are the inner and outer silicon counter arrays (SI), used for tracking and ionisation measurements [10]. Between the two is a cylindrical drift chamber (the Jet Vertex Detector or JVD) [11]. Outside these is the Transition Radiation Detector (TRD) [12], consisting of two sets of radiators and proportional chambers, able to distinguish electron tracks from those of hadrons. The particles were tracked onto the calorimeter surface by the Scintillating Fibre Detector (SFD) [13], which consists of fibres arranged on cylinders into 6 stereo triplets, followed by a 1.5 radiation length thick lead converter covering the full acceptance of the central calorimeter, and a further 2 stereo triplets used as a preshower detector. Electromagnetic showers initiated in the lead converter were detected using the preshower detector.

The central tracking and preshower detectors are completed in the forward regions by the End Cap Proportional Tubes (ECPT) [14].

The position of the event vertex and the directions of the charged tracks were reconstructed using the SFD in conjunction with the SI and the JVD. The fraction of vertices within 300 mm of the detector centre was measured to be $\varepsilon_V = 98 \pm 1\%$. The tracking efficiency for isolated high energy tracks was measured to be $\varepsilon_{trk} = 90.6 \pm 1.1\%$, using a sample of electrons produced in the decay of W bosons ("W electrons").

The outer silicon detector was used to reduce the background from electron pairs arising from photon conversions in the material closer to the beam pipe, and from Dalitz decays. The candidate electron tracks were required to match an outer silicon pad, with measured charge between 0.6 and 1.6 times that expected from a minimum ionising particle. The efficiency of this cut was measured to be $\varepsilon_{sil} = 73.6 \pm 1.1\%$, using W electrons.

The tracking and preshower sections of the SFD were used to match the impact point of candidate electron tracks with the position of electromagnetic showers, with a resolution, measured with W electrons, of $\sigma_{r\phi} = 0.4$ mm in the r-ϕ plane (perpendicular to the beam axis) and $\sigma_z = 1.1$ mm along the beam direction. The quality of a track-preshower match was defined by the variable $d_\sigma^2 = (\Delta_{r\phi}/\sigma_{r\phi})^2 + (\Delta_z/\sigma_z)^2$ where $\Delta_{r\phi}$, Δ_z are the displacements between the track and shower positions. Accidental overlaps between photon showers and charged tracks generally give large values of d_σ^2, while candidate electrons were required to have $d_\sigma^2 < 25$. Preshower clusters for electron candidates were required to have a charge, detected in each of the stereo views of the preshower detector, of at least twice that expected from a minimum ionising particle. The efficiency of the track-preshower matching with the above cuts was measured to be $\varepsilon_{ps} = 89.9 \pm 1.1\%$, using W electrons.

3.3 The Trigger System

The trigger system consisted of 3 levels [15], based on calorimeter information and signals from the Time of Flight counters (TOF, see Fig. 2), which were used to generate a minimum bias trigger signal. The first level trigger used analogue sums of the signals from the photomultipliers of the calorimeter cell compartments up to $|\eta| = 2$. At the second level, electron and jet clusters were reconstructed in a fast processor using information from a fast digitisation of the calorimeter cell signals. A full calorimeter reconstruction was performed in the third level processors, using the full digitisation and a complete set of calibration constants.

Two data samples were used in the analysis. The first was taken from a total of 2.7 pb^{-1} (1.2×10^6 triggers) of data collected during the 1988 run, and consisted of all events containing an electromagnetic cluster with a transverse energy (E_T) above 12 GeV. This

gave a trigger rate of ≈ 1 Hz at a luminosity of 2×10^{30} cm^{-2}s^{-1}. The second sample was a subset of 3×10^5 triggers taken from 4.4 pb^{-1} of data collected during the 1989 run with a trigger using the above cut, as well as requiring an additional calorimeter cluster with E_T above 6 GeV and a missing transverse momentum $\not{p}_T^{raw}$ greater than 9.5 GeV/c reconstructed online :

$$\not{p}_T^{raw} = | \Sigma \, (E_T^{cell} \cdot \vec{u}_{cell})| ,$$

where E_T^{cell} is the sum of the electromagnetic and hadronic transverse energies measured in each cell, weighted with the appropriate correction factors defined in section 3.1, $\vec{u}_{cell}$ is a unit vector in the transverse plane from the centre of the detector to the cell centre, and the sum extends over all calorimeter cells. These additional cuts reduced the third level trigger rate to ≈ 0.1 Hz.

4. SELECTION OF THE TOP CANDIDATES

4.1 Electron Identification

Electron candidates were selected by searching for a track and preshower signal, matching within a tolerance of $d_\sigma^2 < 25$, facing an electromagnetic cluster. The lateral and longitudinal profiles of this cluster were required to be consistent with those expected for a single isolated electron incident along the track direction, by constructing a quality factor $P(\chi^2)$ using extensive test beam measurements. Candidates with $P(\chi^2) < 0.01$, or an energy greater than 1 GeV in the second hadronic compartment, were rejected. The efficiency of this cut was measured to be $\varepsilon_{P(\chi^2)} = 88.7 \pm 0.6\%$ for W electrons.

Combining all the quoted efficiencies, we obtain the overall efficiency to find a W electron with these cuts :

$$\varepsilon_e{}^W = \varepsilon_{cal} \, \varepsilon_v \, \varepsilon_{trk} \, \varepsilon_{sil} \, \varepsilon_{ps} \, \varepsilon_{P(\chi 2)} = 47.6 \pm 1.6\% \, .$$

Using extensive test beam measurements, the measured electron energy was corrected for variations in response over the calorimeter cell surfaces, and for energy lost in the preshower lead converter or cracks between cells. Only candidates with a transverse momentum $p_T^e > 12$ GeV/c were retained.

4.2 *Efficiency of the Electron Selection Cuts in Top Events*

Top events are expected to have more complex topologies and lower energy electrons than the W events, which were used to determine the above efficiency of the electron cuts. The relative efficiency was therefore determined for each cut :

- The cuts used to define an electromagnetic cluster have a lower efficiency (ε_{cal}) for top events, depending upon the process considered and the top quark mass. For example, Monte Carlo studies show that the relative efficiency is approximately 80% for $t\bar{t}$.
- The relative efficiency of the cut on the shower quality factor $P(\chi^2)$ was studied by Monte Carlo simulations of top events, and was found to be 94% to 99%, again depending upon the process and the top quark mass.
- The relative efficiency of the matching between tracking and preshower detectors was studied using W electrons with underlying events with large transverse energy or high charged track multiplicity. It was measured to be 97 ± 3%.
- A relative efficiency of 98 ± 1% was estimated from test beam data, due to a drop in the response of the preshower detector for lower energy electrons.

Combining the above estimates with the overall efficiency to find a W electron with these cuts gives the efficiency to find electrons, in the central calorimeter and with p_T^e above 12 GeV/c, in semi-electronic top decays, as shown in Table 1 as a function of the top mass. The relative error on the efficiencies quoted in this table was estimated to be ±7%, taking into account systematic uncertainties.

Table 1: Estimated Electron Selection Efficiencies for Various Top Masses

m_{top} GeV/c^2	30	40	50	60	63	65	67	70
Efficiency for $t\bar{b}$ %	35.3	38.7	40.2	40.5	41.1	41.4	41.4	41.4
Efficiency for $t\bar{t}$ %	36.1	35.6	35.0	34.4	34.2	34.1	33.9	33.8

4.3 Neutrino Identification

After reconstructing the event vertex and identifying the electron candidate, the missing transverse momentum was recomputed as :

$$\not{p}_T = | \vec{p}_T^{\,e} + \Sigma E_T^{cell} \cdot \vec{u}_{cell} | ,$$

where $\vec{p}_T^{\,e}$ is the reconstructed electron transverse momentum vector, E_T^{cell} is now the cell transverse energy corrected for the position of the vertex, and the sum extends over all cells not used in the electron definition.

A useful variable for discriminating between various classes of events is the transverse mass of the electron-$\not{p}_T$ system :

$$M_T = \sqrt{2}\ p_T^e\ \not{p}_T\ (1-\cos\Delta\phi_{e\nu}) ,$$

where $\Delta\phi_{e\nu}$ is the azimuthal angle between the electron and $\not{p}_T$ vectors. The distribution of $\not{p}_T$ versus M_T is shown in Fig. 3 for the unbiased 1988 sample (no selection on missing transverse momentum applied). The accumulation of events at low $\not{p}_T$ and low M_T is due to background processes in which a hadronic jet fakes the electron signature. The $\not{p}_T$ distribution of these events is shown in Fig. 4. Detector resolution effects, or particles escaping the acceptance, can give rise to a small momentum imbalance. In order to select the events with high energy neutrino emission, only events with $\not{p}_T > 15$ GeV/c were retained. To avoid any trigger bias in comparing the two samples presented in section 3.3, a more stringent cut than that used in the trigger in the 1989 run was made, rejecting events with $\not{p}_T^{raw} < 11$ GeV/c.

4.4 Jet Identification

Any cluster failing to pass the electron cuts was considered to be a jet and its energy was defined as the sum of the cell energies of all cells in the cluster. In this analysis only jets with $|\eta| < 2.2$ were retained, in order to reduce the background from QCD processes for which the jet angular distribution peaks at large pseudorapidity. Events in which the highest transverse energy jet (jet1) was below 10 GeV were rejected.

At this stage the data sample still contained 2 jet events in which a jet fakes the electron signature. Events were removed, in which the difference in azimuth between the electron and the highest energy jet, $\Delta\phi_{e\text{-}jet1}$, was such that :

$$\Delta\phi_{e\text{-}jet1} > 160^{o}.$$

After all the above cuts a total of 58 events were selected from the 1988 data sample, and 79 events from 1989. The M_T distribution for the combined sample of 137 events is shown in Fig. 5.

5. ESTIMATION OF THE EXPECTED SIGNAL

5.1 Monte Carlo Simulation of Top events

The acceptance for top events and their expected M_T distribution were obtained using the Eurojet Monte Carlo program [16], which contains the correct matrix elements for higher order tree level processes in heavy quark production (order α_s for $t\bar{b}$ and order α_s^3 for $t\bar{t}$).

The presence of these higher order processes increases the acceptance for top events, since they lead to final states with additional jets. The fact that the theoretical calculation is not complete to all orders should result in an underestimate of the acceptance for events containing an electron and a jet in the final state. The calculation is regularised using a cutoff of 5 GeV on the E_T of additional partons in the higher order terms. The acceptance was not significantly changed if this cutoff was varied between 2 and 7 GeV.

The top quark decay in Eurojet was simulated after hadronisation into a top meson or baryon. The branching fractions used were those expected in the Standard Model for a free quark decay, 1/9 for each of the three semi-leptonic decays (b-hadron plus a lepton and its neutrino), and 1/3 for each of the two non-leptonic decays (b-hadron plus a light quark-antiquark pair). The fraction z of the top quark momentum carried by the top hadron was drawn from the parameterisation of [17] :

$$f(z)dz = N\, dz \,/\, \left\{ z\,[1\text{-}1/z\text{-}\varepsilon_q\,/(1\text{-}z)]^2 \right\} ,$$

where N is a normalisation factor and $\varepsilon_q = (m_q/m_{top})^2$, with m_q the mass of the light quark in the top hadron. Given the large values of m_{top} considered, the exact value of ε_q did not affect the results.

The bottom and charm hadron decays were generated using extrapolations from known exclusive branching ratios, and the simulations were insensitive to the exact values used. After reconstruction in the UA2 calorimeter, jets from hadronic bottom decays were very similar to those from gluons of the same initial parton energy, and only slightly broader than those from light quarks.

Gluons were fragmented into light quark pairs, each with an average p_T relative to the gluon direction, b = 0.4 GeV/c, and light quark fragmentation followed the parameterisation of Field and Feynman [18] :

$$f(z) = 1 - a + 3a\,(1 - z)^2\,,$$

where, at each step of the fragmentation, z is the fractional longitudinal momentum carried by the generated hadron, which has a p_T distributed with an average value, b = 0.4 GeV/c. The value of the parameter a = 0.89 was chosen to agree with UA1 data on jet fragmentation [16].

Finally a full simulation was performed of the calorimeter response to all the generated particles, using extensive test beam measurements with hadron and electron beams, over an energy range from 300 MeV to 150 GeV. As far as possible, the Monte Carlo events were then analysed in the same way as the data.

5.2 Systematic Errors in the Acceptance

Several sources of systematic error in the acceptance were studied.

- In all cases, the underlying event generated by the Eurojet Monte Carlo program was replaced by the energy pattern of minimum bias events measured in UA2. It was found that a reasonable simulation of the transverse energy accompanying W electrons was obtained by using the superposition of two minimum bias events. The systematic error on the acceptance for top events due to this procedure was estimated by using the results obtained using one or three minimum bias events as the underlying event for the generated top signal, and was found to be ±4% for $t\bar{b}$ and ±2% for $t\bar{t}$, for a top mass of 65 GeV/c^2.
- The calorimeter response to jets is very sensitive to the response to low energy hadrons (< 1GeV). The measured response curve was adjusted to give the lowest response consistent with the test beam data, thus reducing the acceptance for events with at least one jet with E_T > 10 GeV. The uncertainty in the absolute energy scale of the calorimeter (±1% in the electromagnetic and ±2% in the hadronic compartments) was

also taken into account by adjusting the response downwards. In the worst case the relative loss in acceptance was 5% for $t\bar{b}$ and 2% for $t\bar{t}$ for a top quark mass of 65 GeV/c^2, the difference being due to the higher jet multiplicity in the $t\bar{t}$ final state.

- The parameters a and b used in the fragmentation functions were varied within limits consistent with the observed energy flow in jets with $E_T \approx 10$ GeV measured in UA2. In the worst case the loss in acceptance was 2% for both production processes.

A lower limit on the acceptance was obtained by simultaneously setting each of the above parameters within its range so as to minimise the acceptance.

5.3 Production Cross Sections

Table 2 gives the production cross sections ($\sigma_{t\bar{b}}$ and $\sigma_{t\bar{t}}$) used (see Section 2, Fig. 1). For $\sigma_{t\bar{b}}$ the lower limit in brackets was obtained assuming $m_W = 79.8$ GeV/c^2, one standard error lower than the value of 80.2 ± 0.4 GeV/c^2, obtained by combining the best value of the Z boson mass [19] with the average of low energy measurements of $\sin^2\theta_W$ [1]. Because of the small available phase space, this change has a significant effect on $\sigma_{t\bar{b}}$, for top masses above 60 GeV/c^2. In the case of $\sigma_{t\bar{t}}$ the lower limit in brackets was taken from [6], corresponding to about 70% of the central value.

Table 2 : Estimated Acceptance and Signal Rates for Various Top Masses

m_{top}	Cross section (pb)		Acceptance (%)		Expected events	
GeV/c^2	$t\bar{b}$	$t\bar{t}$	$t\bar{b}$	$t\bar{t}$	All M_T	$15 < M_T < 50$
30	1522 (1522)	3040 (2128)	1.8 (1.5)	1.9 (1.7)	39.2 (26.2)	33.4 (22.4)
40	1211 (1211)	643 (450)	4.1 (3.5)	7.1 (6.4)	39.2 (28.3)	34.9 (25.4)
50	845 (820)	188 (132)	8.1 (7.1)	16.8 (15.3)	38.2 (28.9)	34.4 (26.2)
60	459 (436)	66.9 (46.8)	12.3 (11.0)	25.2 (22.9)	26.7 (20.8)	22.6 (17.6)
63	349 (328)	50.3 (35.2)	12.1 (10.8)	29.6 (27.0)	21.3 (16.3)	17.0 (13.3)
65	283 (263)	40.9 (28.6)	12.4 (11.1)	29.5 (26.9)	17.6 (13.4)	13.6 (10.6)
67	218 (200)	34.4 (24.1)	12.5 (11.1)	32.4 (29.5)	14.5 (10.8)	11.0 (8.2)
70	136 (122)	26.7 (18.7)	15.3 (13.6)	35.5 (32.3)	11.5 (8.5)	8.3 (6.2)

5.4 Results on Acceptances

Also shown in Table 2 are the acceptances obtained for each process, defined as the fraction of generated top events with a semi-electronic top quark decay, which pass the kinematic cuts defined in section 4 :

$$p_T^e > 12 \text{ GeV/c}, \not{p}_T > 15 \text{ GeV/c}, E_T^{jet1} > 10 \text{ GeV, and } \Delta\phi_{e\text{-jet1}} < 160^o.$$

In each case the central value is given, followed (in brackets) by the lowest value consistent with the systematic errors, as discussed above. Because the transverse energy spectrum of jets from top decays is soft and because the largest contribution to a possible signal from top quark production arises from the $t\bar{b}$ process, which has smaller jet multiplicities in the final state, we note that the acceptances quoted in Table 2 would be significantly reduced if we would require at least two jets to pass the E_T threshold.

The acceptance increases for $t\bar{t}$ as the top quark mass increases, since the decay products all have increasing average E_T. The acceptance variation for $t\bar{b}$ as a function of the top quark mass is more complicated, due to the smaller number of jets in the final state, and the decreasing average E_T of the $\bar{b}$ jet as the top quark mass increases. The acceptance is lower for $t\bar{b}$ compared to $t\bar{t}$, partly because the top quark is assumed to be polarised in the $t\bar{b}$ case, with a polarisation which decreases when the top quark mass increases, and unpolarised in $t\bar{t}$. This is a conservative assumption since fragmentation effects such as gluon emission and hadronisation are expected to reduce the polarisation and increase the acceptance. There is however no quantitative theoretical prediction of these effects.

Table 2 also gives the number of events expected from both processes after taking into account the electron detection efficiencies of Table 1 and the semi-leptonic branching ratio. The lower limit (in brackets) on the number of events uses the lower production cross sections and the lower limits on the acceptances given in Table 2. The errors on the integrated luminosity (7.1 ± 0.5 pb^{-1}), on the observed number N_W of $W \rightarrow e\nu_e$ decays, on the electron cut efficiency, and on the number of Monte Carlo events, which are not included in Table 2, were treated as independent Gaussian errors in the determination of the top quark mass limit (section 7), and did not significantly affect the final result. The expected number of events is also given for the transverse mass range $15 < M_T < 50$ GeV/c^2, where most of the signal is expected. As an example the transverse mass distribution predicted for a top quark mass of 65 GeV/c^2 is given in Fig. 6a.

6. BACKGROUND PROCESSES

6.1 $W \rightarrow e\nu_e$ *and* $W \rightarrow \tau\nu_\tau, \tau \rightarrow e\nu_e\nu_\tau$

The main source of associated high energy electrons and neutrinos in the Standard Model is W boson production and decay via :

$$W \rightarrow e\nu_e \quad \text{or} \quad W \rightarrow \tau\nu_\tau, \tau \rightarrow e\nu_e\nu_\tau .$$

These events ("W events") will enter the data sample of Fig. 5, if the W boson is produced in association with a high E_T jet. The Jacobian peak expected from W events can clearly be seen in the $\not{p}_T$ distribution of the data (Fig. 4). The transverse mass distribution expected for such events was modelled using the EKS Monte Carlo program [20], which includes a complete tree level calculation up to order α_s^3, and is shown in Fig. 6b, for both the $W \rightarrow e\nu_e$ and the $W \rightarrow \tau\nu_\tau, \tau \rightarrow e\nu_e\nu_\tau$ contributions. The underlying event was again simulated by using the superposition of two minimum bias events from the data. Since the transverse mass, M_T, depends only on the electron and the missing transverse momentum, it is only indirectly sensitive to details of the event associated to the W such as the number of jets or the jet fragmentation model used.

The absolute normalisation for the EKS prediction is poorly known, when one or more jets are required in association with the $W \rightarrow e\nu$ decay, and depends on higher order QCD corrections, fragmentation functions, and the details of the simulation of the detector response to jets. The normalisation was therefore taken from the 105 events observed in Fig. 5 with $M_T > 60$ GeV/c^2, where little top signal is expected, which gives an expectation of 148.5 ± 14.5 events over the full M_T range. The EKS prediction is found to be low by a factor 1.3 ± 0.5, consistent with one within the large theoretical and experimental uncertainties quoted above.

6.2 $Z \rightarrow ee$

Decays of the Z boson into an electron pair can simulate missing p_T if one of the electrons is misidentified as a jet. The electromagnetic part of its energy is then multiplied by the correction factor for hadrons, thus generating a spurious momentum imbalance. This process was also simulated using the EKS Monte Carlo program which predicts a total of 1.7 ± 0.5 events passing the cuts. Since the electron, "jet" and missing transverse momentum are all due to the e^+e^- pair in the final state, this estimate does not depend on QCD corrections or jet simulation. In order to check this estimate, the cut on $\Delta\phi_{e\text{-jet1}}$ was

removed and all the events were inspected for Z candidates. A total of 14 candidates were found compared to the Monte Carlo prediction of 15 ± 3 events.

6.3 $Z \rightarrow \tau\tau, \tau \rightarrow e\nu_e\nu_\tau, \tau \rightarrow \nu_\tau X$

This process can also give rise to the required signature, although the p_T spectrum of the electron is softer than in the previous case. The EKS Monte Carlo program was used to estimate the total background from this source to be 0.8 ± 0.3 events.

6.4 $p\bar{p} \rightarrow b\bar{b} + X, b \rightarrow e\nu_e c$

This process produces electrons by semileptonic b decay in association with a charm quark which fragments into hadrons. The electron will therefore be non-isolated and will normally fail to pass the initial trigger cuts on the electromagnetic shower profile, or the cut on $P(\chi^2)$ which is derived using isolated electrons. The efficiency for electrons from b decays was estimated to be 5 ± 2% of that for electrons from W decays, for events passing the topological cuts. In addition, the recoiling $\bar{b}$ jet will normally fail the cut on $\Delta\phi_{e\text{-jet1}}$. Although neutrinos and muons produced in the decay chains of the heavy quarks will penetrate the calorimeter and give rise to missing p_T, the cut at $\not{p}_T > 15$ GeV/c is rarely satisfied.

A full simulation was performed using the Eurojet Monte Carlo program, with its production cross section normalised using the results of UA1 [21]. The total estimated background was 1.0 ± 0.6 events, where the error includes the uncertainties on the production cross section and the electron efficiency.

6.5 *Jets Misidentified as Electrons*

Most of the electron candidates in events with $\not{p}_T < 10$ GeV/c are misidentified hadronic jets (QCD background). In order to estimate the contribution of this background to the final sample ($\not{p}_T > 15$ GeV/c and $E_T^{jet1} > 10$ GeV), events were selected which failed the electron cuts. The events with $\not{p}_T < 10$ GeV/c, from the unbiased 1988 data, were used to normalise the samples relative to each other. The amount of QCD background in the final sample with $\not{p}_T > 15$ GeV/c and $E_T^{jet1} > 10$ GeV was obtained by using the same normalisation factor. The transverse mass distributions of the electron candidate and background samples with $10 < \not{p}_T < 15$ GeV/c were in good agreement.

The estimate of the QCD background was 2.4 ± 1.5 events, where the error includes systematic uncertainties due to the assumptions made in the estimate. The QCD background for $M_T > 50$ GeV/c^2 was estimated to be negligible.

6.6 Summary of the Background Estimates

The various background contributions to the event sample are given in Table 3. Since the top signal is expected to concentrate at intermediate values of M_T, the values are also given for the region $15 < M_T < 50$ GeV/c^2.

Table 3 : Summary of the Event Sample and Expected Backgrounds

	All M_T	$15 < M_T < 50$ GeV/c^2
$Z \rightarrow ee, \tau\tau$	2.5 ± 0.6	1.6 ± 0.5
$b\bar{b}$	1.0 ± 0.6	0.5 ± 0.3
QCD	2.4 ± 1.5	2.1 ± 1.5
Total of above backgrounds	5.9 ± 1.7	4.2 ± 1.6
W events	148.5 ± 14.5	22.0 ± 3.0
Total Background	154.4 ± 14.6	26.2 ± 3.4
Observed Events	137	17

7. LIMITS ON THE TOP MASS

From the numbers shown in Table 3, we conclude that there is no indication for a signal from the top quark in the sample. For a top quark mass of 65 GeV/c^2, a lower limit of 10.6 events would be expected in the range $15 < M_T < 50$ GeV/c^2 (Table 2). Using a simple calculation based on Poisson statistics, accounting for the error on the background estimate [22], this hypothesis is excluded at the 98.6% confidence level.

Limits on the top mass were obtained by comparing the M_T distribution of the observed events with that expected from background sources alone, or in the presence of a top signal of given mass. The M_T distribution for W events was taken from Fig. 6b. The exact shape

of the M_T distribution for other background sources was uncertain, mainly due to the small number of events found in each background sample. However, the results were insensitive to the exact shape of the background distribution. The expected signal distribution was taken from the Eurojet Monte Carlo program using the appropriate top mass; for example the distribution of Fig. 6a was used for a top mass of 65 GeV/c^2.

A likelihood fit was then performed to the observed events with two free parameters, corresponding to the fraction of the event sample due to top decays and to W events. The normalisation of background sources other than W events was imposed from the estimates quoted in Table 3. The total likelihood function normalisation was constrained, within Poisson statistics, to the total number of 137 observed events in the data sample. The 90 and 95% confidence limits on the number of top events in the sample were obtained by integrating the likelihood distribution over all possible values of the signal.

For each top mass considered, the fitted signal was consistent with no top production. Fig. 7 shows the best fit to the data with no top contribution. The lower limit contribution of 13.4 events from top, for a top quark mass of 65 GeV/c^2 (Table 2), is superimposed to the result of this fit. The likelihood fit excludes this hypothesis at the 99.0% confidence level. This does not significantly improve the result based on the observed rate of events in the transverse mass range $15 < M_T < 50$ GeV/c^2, quoted above. We have also checked that our results do not significantly improve if we include other variables, such as the jet multiplicity or the jet angular distributions.

Fig. 8 shows the total expected cross section for top production, as a function of the top quark mass, using the lower limit cross sections quoted in Table 2. Also shown are the 90 and 95% confidence level cross sections excluded by the fit. Top quark masses between 30 and 69 (71) GeV/c^2 are excluded with 95 (90)% confidence. Given the existing lower limits on the top quark mass [2,3], values below 30 GeV/c^2 were not considered in this analysis.

The fit procedure takes into account the large error on the estimate of the background sources. Setting the total background equal to the number of observed events would reduce the above limits by approximately 4 GeV/c^2. Using the central values for the acceptance and production cross sections would increase the limits by approximately 3 GeV/c^2.

Since the acceptance is different for top production mediated by the W boson and by QCD processes, the limits of Fig. 8 are only valid for the cross sections used above. In order to display the limits which would be obtained for other assumptions, for example an improved

calculation of the $t\bar{t}$ production cross section, Fig. 9 shows the plane $\sigma_{t\bar{b}}$ versus $\sigma_{t\bar{t}}$, where the two cross sections are normalised to the central values of the measurement of [4] and the calculations of [6] respectively. The regions excluded at 95% confidence level, including the experimental systematics, are shown for various values of the top quark mass. For example, we would exclude top quark masses between 34 and 66 GeV/c^2, if the top quark were produced through electroweak processes alone ($\sigma_{t\bar{t}} = 0$), and if the lower limits of Table 2 are taken for $\sigma_{t\bar{b}}$. Figure 9 also shows that our results are not very sensitive to the exact value of the $t\bar{t}$ cross section. In particular, the 95% confidence level limit on the top quark mass of 69 GeV/c^2, obtained from Fig. 8, increases only by 1 GeV/c^2 if we use the central prediction for $t\bar{t}$ production. Recent results form the Fermilab Tevatron Collider, based only on $t\bar{t}$ production, which is dominant at $\sqrt{s}$ = 1.8 TeV, exclude $40 < m_{top} < 77$ GeV/c^2 at 95% confidence [23].

8. LIMITS ON THE b' MASS

Figure 9 can also be used to extract a mass limit on a hypothetical member of a new quark family (b'), assuming that its partner is too heavy to allow production mediated by the weak interaction and that its decay matrix element is identical to that of a top quark. The excluded region in Fig. 9, for $\sigma_{t\bar{b}} = 0$, gives $m_{b'} > 53$ (56) GeV/c^2 at 95 (90) % confidence.

We have redone this analysis, using the correct matrix element for the b' decay, and assuming that the b' branching ratio to a charm quark and a virtual W boson is 100%. The acceptances were found to be larger in this case than for t decay, mainly because of the harder electron spectrum obtained and of the better detector response to charm quark jets than to bottom quark jets. We thus obtain $m_{b'} > 54$ (57) GeV/c^2 at 95 (90) % confidence.

9. CONCLUSIONS

A search has been performed for evidence for production and decays of top quarks or b' quarks with the upgraded UA2 detector at the CERN $\bar{p}p$ Collider. No evidence was found for such processes, leading to new lower limits on the top and b' quark masses, assuming standard branching ratios :

$m_{top} > 69$ GeV/c^2, $m_{b'} > 54$ GeV/c^2 at the 95 % confidence level,

and

$m_{top} > 71$ GeV/c^2, $m_{b'} > 56$ GeV/c^2 at the 90 % confidence level.

ACKNOWLEDGEMENTS

We gratefully acknowledge P.Darriulat for his contributions and guidance during the design and construction of the UA2 upgrade project.

The technical staff of the institutes collaborating in UA2 have contributed substantially to the construction and operation of the experiment. We deeply thank them for their continuous support. The experiment would not have been possible without the very successful operation of the improved CERN $\bar{p}p$ Collider, whose staff and coordinators we sincerely thank for their collective effort.

Financial support is acknowledged from the Schweizerischen Nationalfonds zur Förderung der Wissenschaftlichen Forschung to the Bern group, from the UK Science and Engineering Research Council to the Cambridge group, from the Bundesministerium für Forschung und Technologie to the Heidelberg group, from the Institut National de Physique Nucléaire et de Physique des Particules to the Orsay group, from the Istituto Nazionale di Fisica Nucleare to the Milano, Pavia, Perugia and Pisa groups and from the Institut de Recherche Fondamentale (CEA) to the Saclay group.

REFERENCES

[1] See for example :
J. Ellis and G.L. Fogli, Phys. Lett. B231 (1989) 189, and references therein;
P. Langacker, Phys. Rev. Lett. 63 (1989) 1920.

[2] AMY Collaboration, S. Eno et al., Phys. Rev. Lett. 63 (1989) 1910;
TOPAZ Collaboration, I. Adachi et al., Phys. Lett. 229B (1989) 427;
VENUS Collaboration, K. Abe et al., submitted to Phys. Lett.;
MARKII Collaboration, G.S. Abrams et al., SLAC-PUB-5106 (1989).

[3] UA1 Collaboration, C. Albajar et al., Z. Phys. C37 (1988) 505, as updated by the results of Ref. 6.

[4] UA2 Collaboration, H. Plothow-Besch, Proc. of the 1989 Europhys. Conf. on High Energy Phys. (Madrid), to be published in Nucl. Phys. .

[5] L.J. Reinders et al., Phys. Rep. 127 (1985) 1;
T. Alvarez et al., Nucl. Phys. B301 (1988) 1.

[6] G. Altarelli et al., Nucl. Phys. B308 (1988) 724.

[7] P. Nason, S. Dawson and R.K. Ellis, Nucl. Phys. B303 (1988) 607.

[8] A. Beer et al., Nucl. Inst. and Meth. 224 (1984) 360.

[9] F. Alberio et al., The Electron, Jet, and Missing Transverse Energy Calorimetry of the Upgraded UA2 Experiment at the CERN $\bar{p}p$ Collider, to be published in Nucl. Inst. Meth..

[10] R. Ansari et al., Nucl. Instr. Meth. A279 (1989) 388.

[11] F. Bosi et al., CERN-EP/89-82 (1989).

[12] R. Ansari et al., Nucl. Inst. Meth. A263 (1988) 51.

[13] J. Alitti et al., Nucl. Inst. Meth. A279 (1989) 364.

[14] K. Borer et al., End Cap Proportional Tube Chambers for the Upgraded UA2 Experiment, to be published in Nucl. Instr. Meth. .

[15] G. Blaylock et al., Proc. of the International Conference on the Impact of Digital Microelectronics and Microprocessors on Particle Physics 1988, eds. M. Budinich et al. (World Scientific, Singapore, 1988), p. 247 and 254.

[16] A. Ali and B. van Eijk, Proc. 5th Top. Work. on Proton-Antiproton Coll. Phys., St Vincent, Aosta, Italy (1985);
B. Van Eijk, CERN-EP/85-121 (1985);
A. Ali et al., CERN-TH.4523/86 (1986);
A. Ali et al., Nucl Phys. B292 (1987) 1.

[17] C. Peterson et al., Phys. Rev. D27 (1983) 105.

[18] R.D. Field and R.P. Feynman, Nucl. Phys. B136 (1978) 1.

[19] CDF Collaboration, F. Abe et al., Phys. Rev. Lett. 63 (1989) 720;
MARK II Collaboration, G.S. Abrams et al., Phys. Rev. Lett. 63 (1989) 2173;
ALEPH Collaboration, D. Decamp et al., Phys. Lett. 231B (1989) 519;
DELPHI Collaboration, P. Aarnio et al., Phys. Lett. 231B (1989) 539;
L3 Collaboration, B. Adeva et al., Phys. Lett. 231B (1989) 509;
OPAL Collaboration, M. Akrawy et al., Phys. lett. 231B (1989) 530.
[20] S.D. Ellis, R. Kleiss, and W.J. Stirling, Phys. Lett. 154B (1985) 435;
F.A. Berends et al., Phys. Lett. 224B (1989) 237.
[21] UA1 Collaboration, C. Albajar et al., Z. Phys. C37 (1988) 489.
[22] Particle Data Group, Review of Particle Properties, Phys. Lett. 204B (1988) 81.
[23] CDF Collaboration, F. Abe et al., UPR-0172E (1989).

FIGURE CAPTIONS

Fig. 1 Cross sections for top production in $\bar{p}p$ interactions at $\sqrt{s} = 630$ GeV.

Fig. 2 Partial and schematic longitudinal view of the UA2 detector.

Fig. 3 M_T versus $\not{p}_T$ for events with an electron candidate (1988 data only).

Fig. 4 Distribution of $\not{p}_T$ for events with an electron candidate (1988 data only).

Fig. 5 Distribution of M_T for the final sample.

Fig. 6 M_T distribution for : a) Top decays with $m_{top} = 65$ GeV/c^2 and b) W events.

Fig.7 Best fit (full curve) to the M_T distribution of Fig.5 with no top signal. The lowest expected contribution from top ($m_{top} = 65$ GeV/c^2) is added (dashed curve).

Fig. 8 Lower limit for the top production cross section and the 90 and 95% CL excluded cross sections as a function of m_{top}.

Fig. 9 Limits at 95% CL on top production as a function of $\sigma_{t\bar{b}}$ and $\sigma_{t\bar{t}}$ for various values of m_{top}. The cross section $\sigma_{t\bar{b}}$ is normalised to the measurement of Ref.4 and the cross section $\sigma_{t\bar{t}}$ is normalised to the calculations of Ref.6. The excluded regions lie above the lines represented for each m_{top}, as illustrated by the dashed area for $m_{top} = 70$ GeV/c^2. The cross represents the limit $m_{top} > 69$ GeV/c^2 obtained for the lower values shown in Table 2 for $\sigma_{t\bar{b}}$ and $\sigma_{t\bar{t}}$.

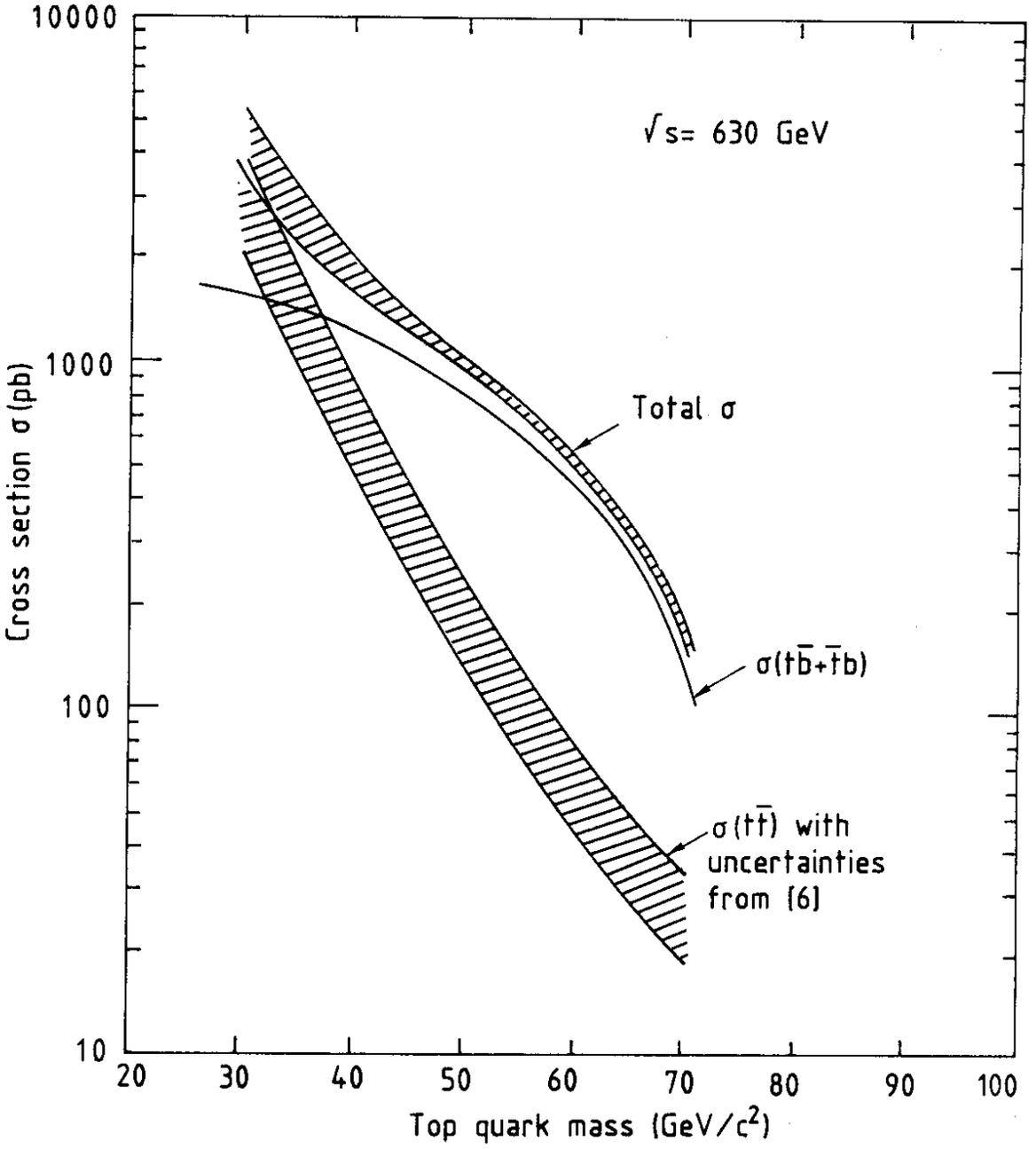
10000
1000
100
10
Cross section σ (pb)
√s= 630 GeV
Total σ
σ(tb̄+t̄b)
σ(tt̄) with
uncertainties
from [6]
20
30
40
50
60
70
80
90
100
Top quark mass (GeV/c²)

Fig. 1

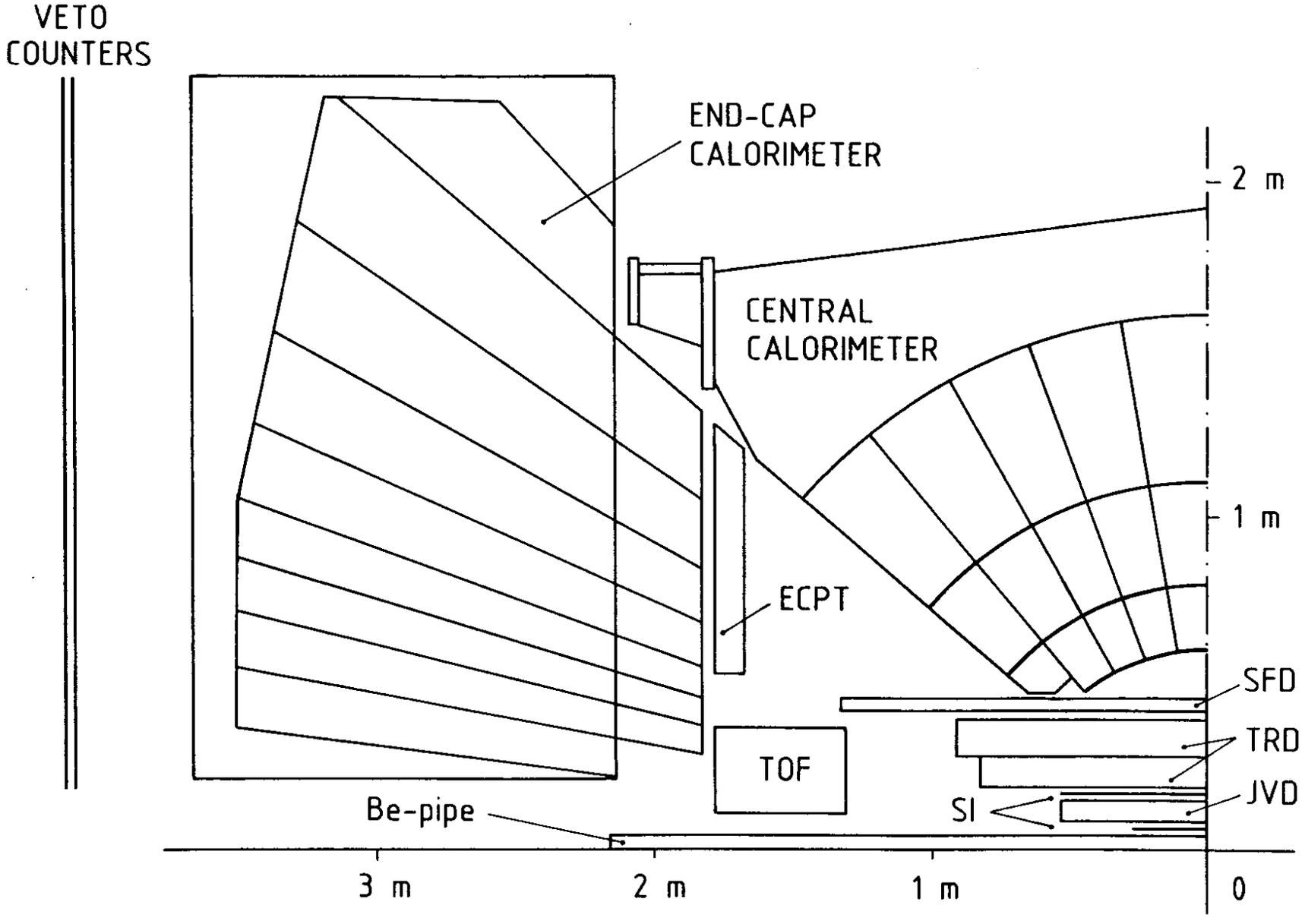
VETO
COUNTERS
END-CAP
CALORIMETER
CENTRAL
CALORIMETER
ECPT
TOF
Be-pipe
SFD
TRD
JVD
SI
2 m
1 m
3 m
2 m
1 m
0

Fig. 2

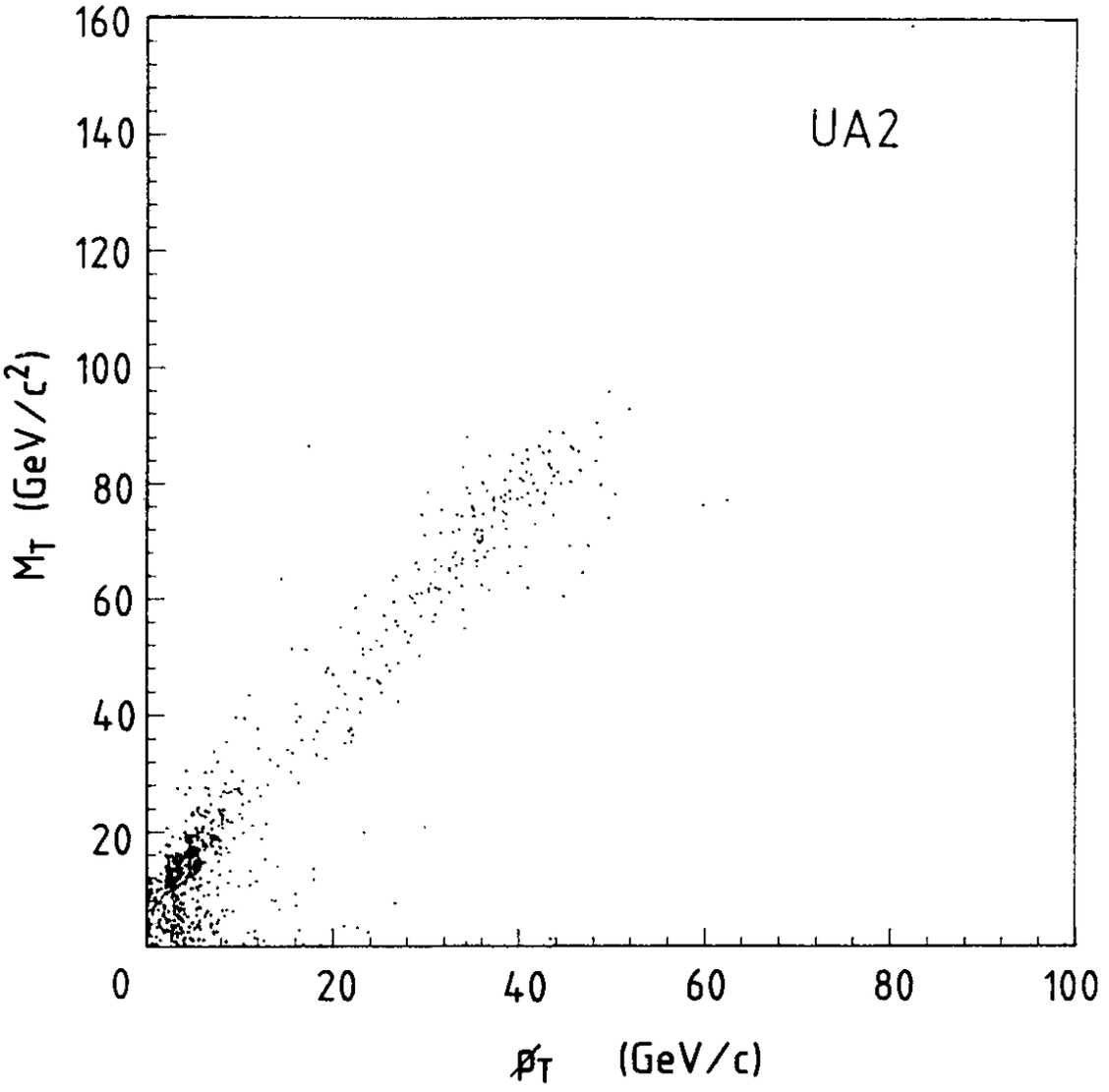
UA2
160
140
120
100
80
60
40
20
0
20
40
60
80
100
M_T (GeV/c^2)
$\not{p}_T$ (GeV/c)

Fig. 3

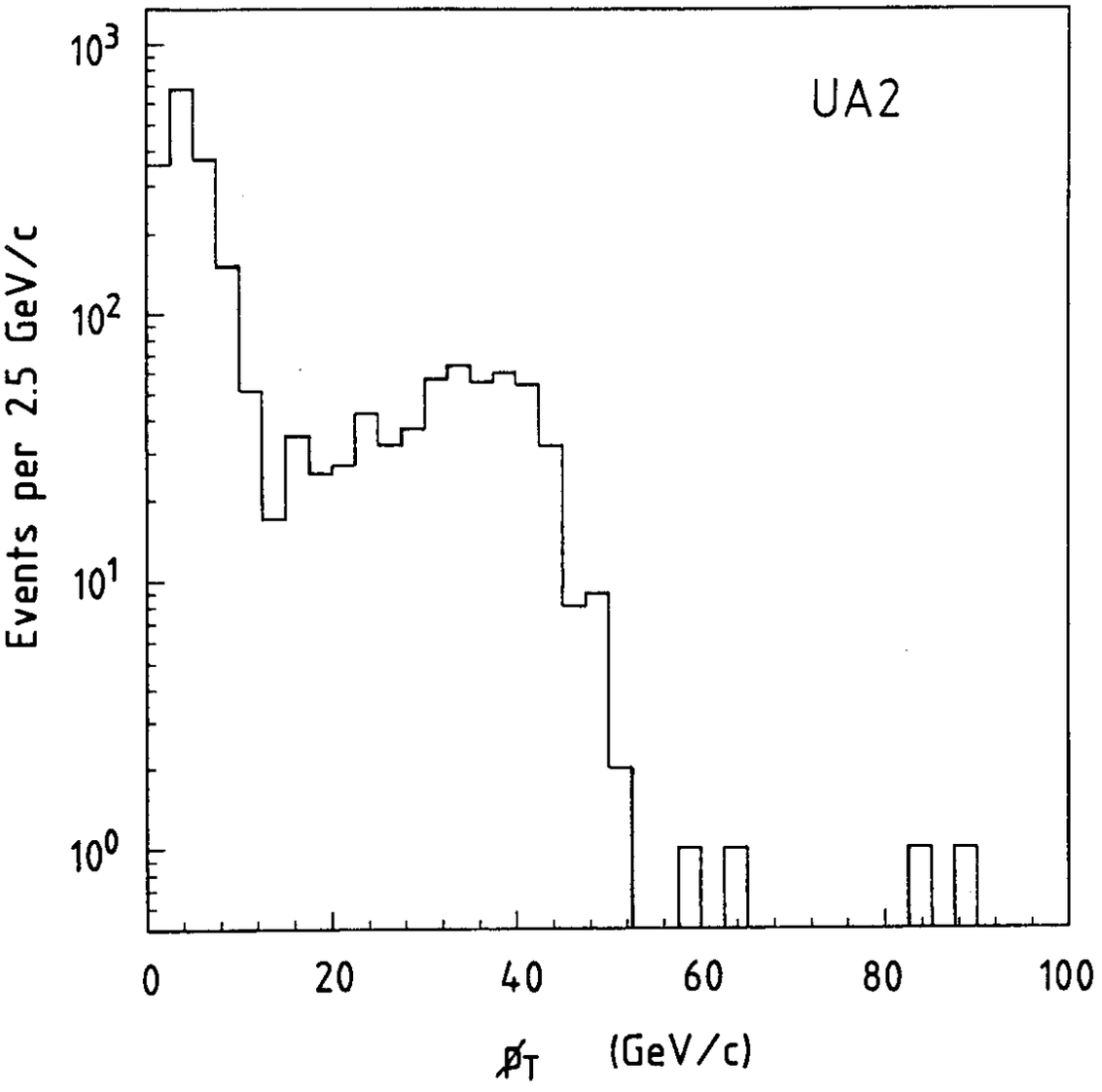
UA2
Events per 2.5 GeV/c
10^3
10^2
10^1
10^0
0
20
40
60
80
100
$\not{p}_T$ (GeV/c)

Fig. 4

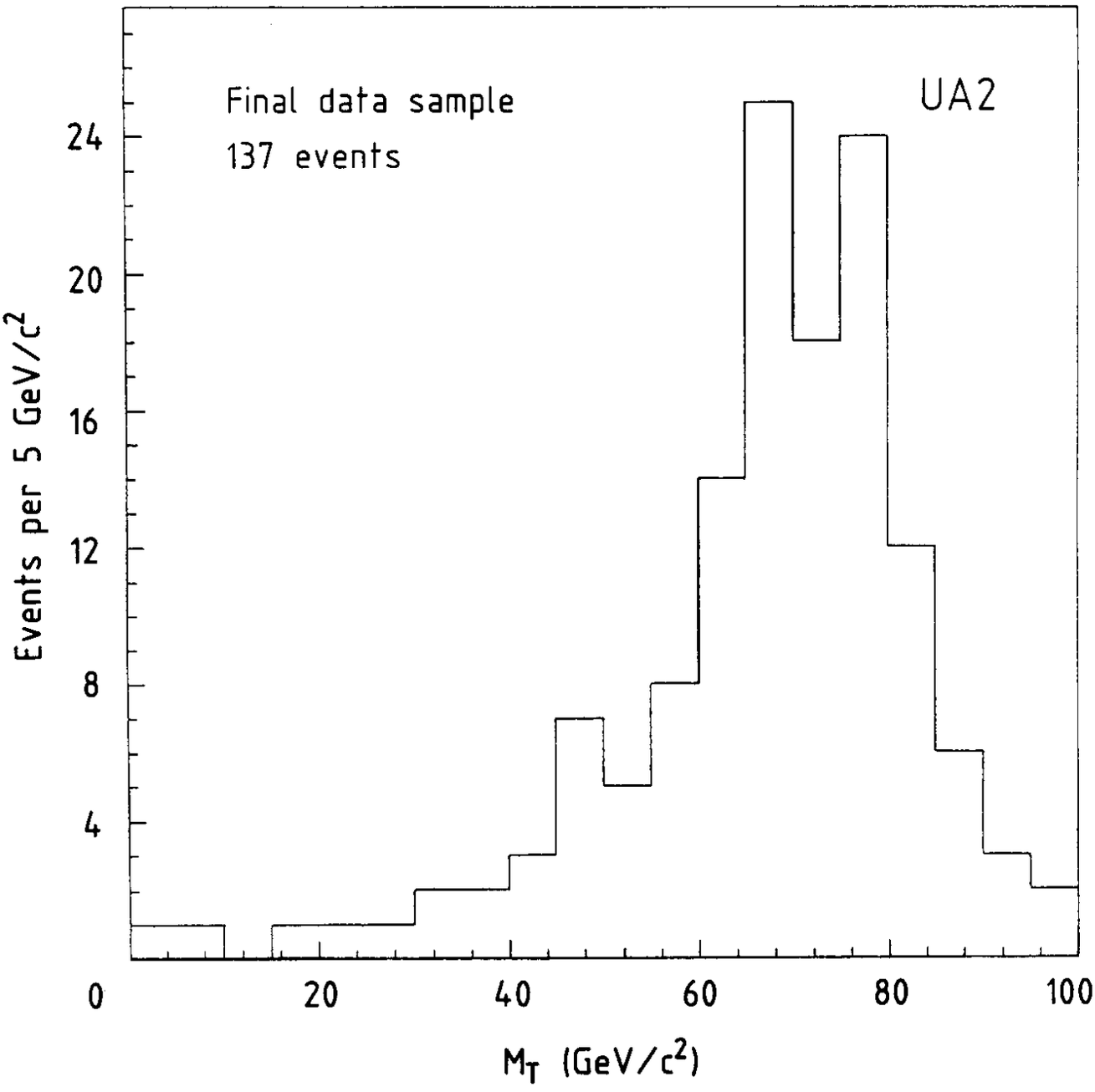
Final data sample
137 events
UA2
Events per 5 GeV/c²
24
20
16
12
8
4
0
20
40
60
80
100
M_T (GeV/c²)

Fig. 5

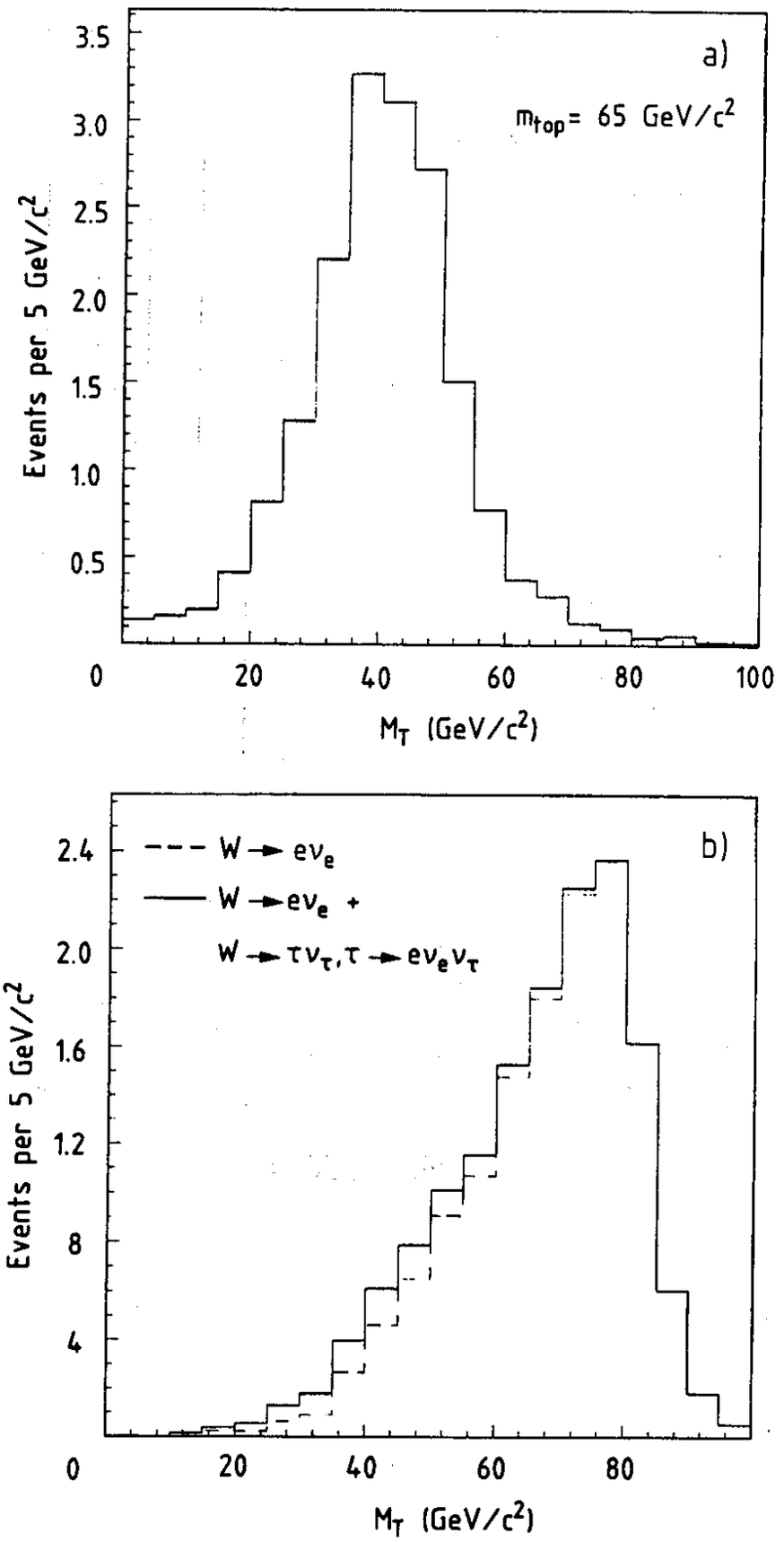
a)
m_{top}= 65 GeV/c^2
Events per 5 GeV/c^2
M_T (GeV/c^2)
b)
W → eν_e
W → eν_e +
W → $\tau\nu_\tau$, τ → e$\nu_e\nu_\tau$
Events per 5 GeV/c^2
M_T (GeV/c^2)

Fig. 6

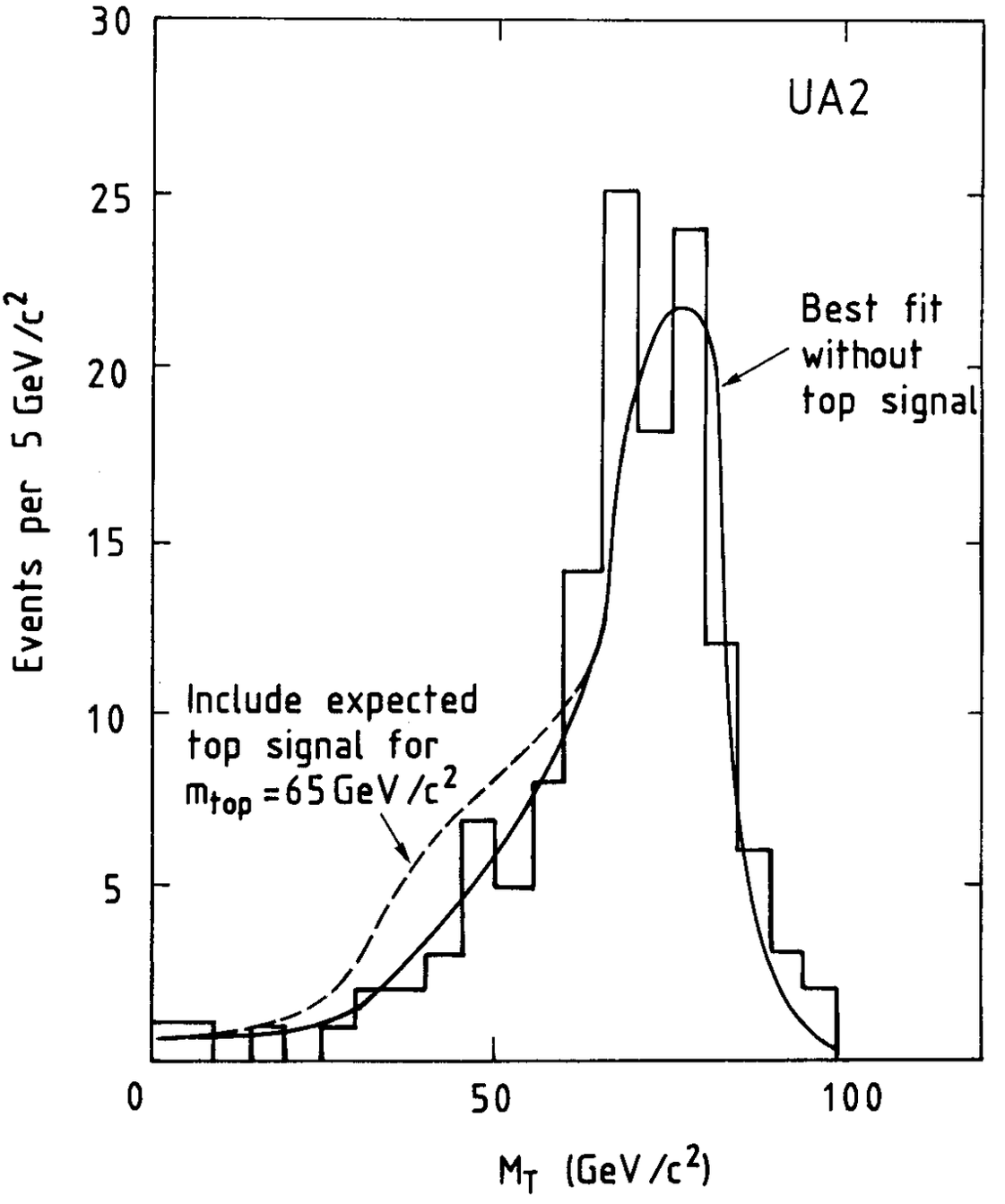
UA2
Best fit
without
top signal
Include expected
top signal for
$m_{top} = 65\,GeV/c^2$
Events per 5 GeV/c²
M_T (GeV/c²)
0
50
100
5
10
15
20
25
30

Fig. 7

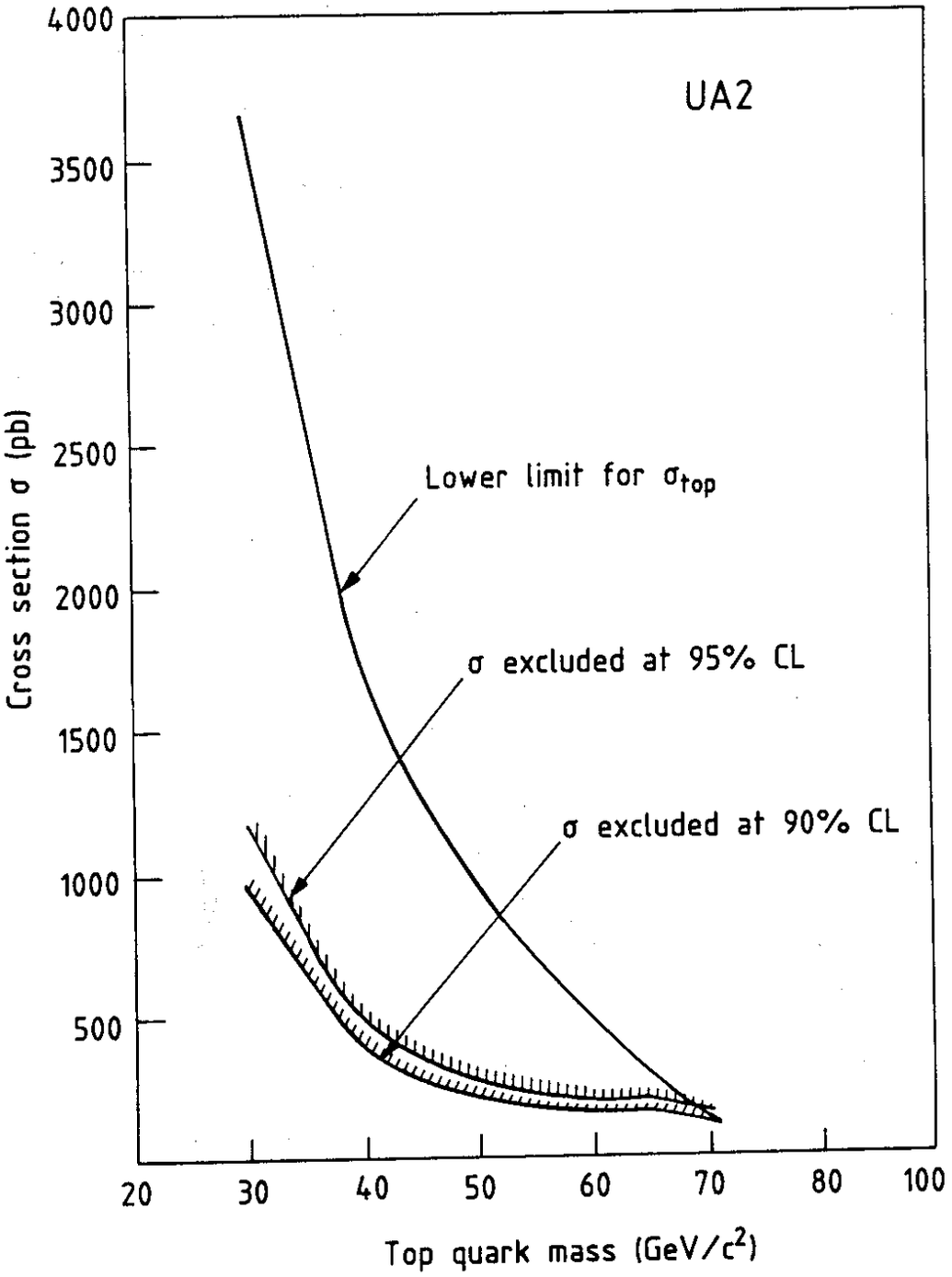
UA2
Lower limit for σ_{top}
σ excluded at 95% CL
σ excluded at 90% CL
Cross section σ (pb)
Top quark mass (GeV/c²)
4000
3500
3000
2500
2000
1500
1000
500
20
30
40
50
60
70
80
100

Fig. 8

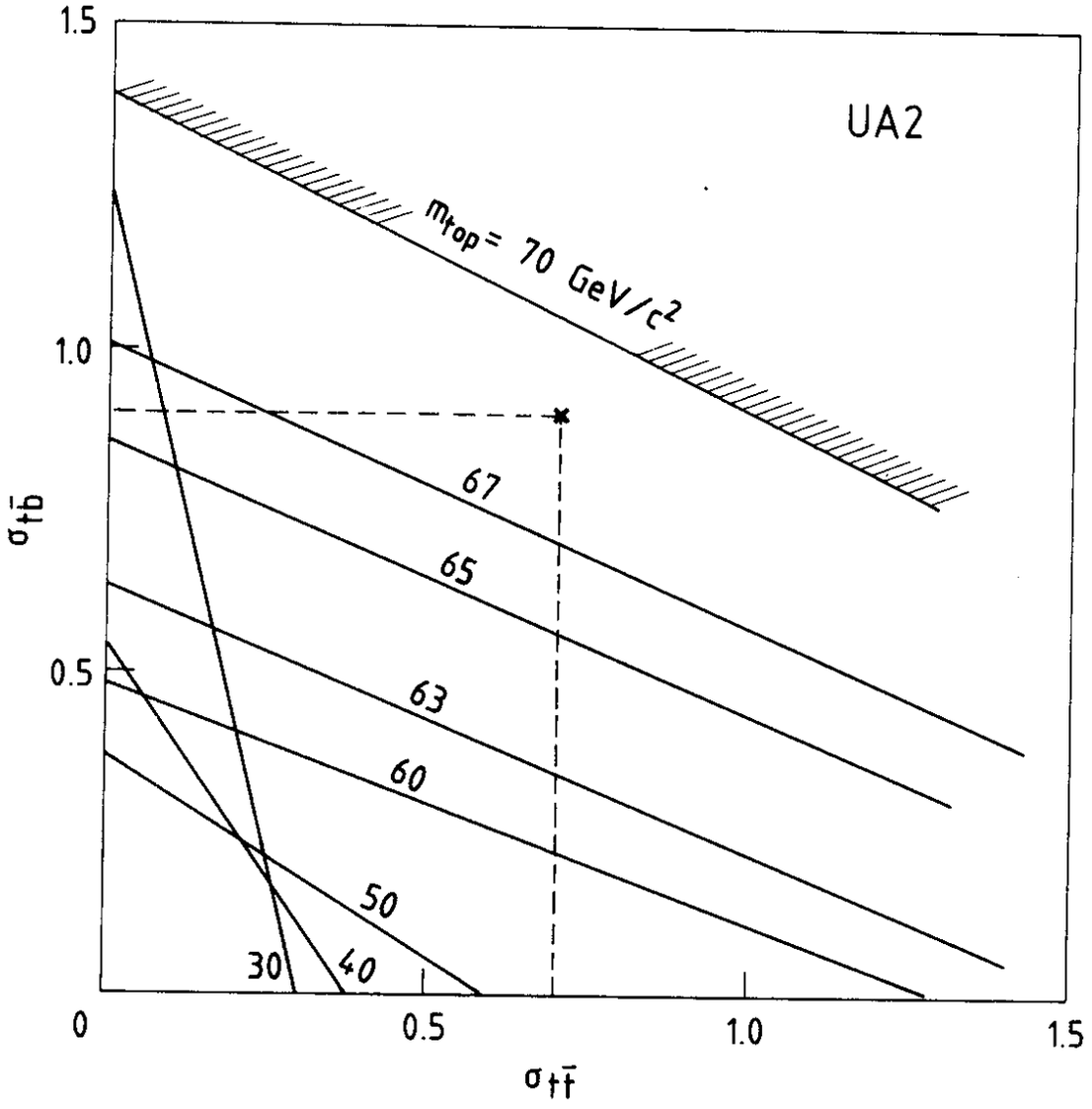
UA2
m_{top} = 70 GeV/c^2
67
65
63
60
50
40
30
1.5
1.0
0.5
0
0.5
1.0
1.5
$\sigma_{t\bar{b}}$
$\sigma_{t\bar{t}}$

Fig. 9